

Fig. 2: $SC(3,2)$ and $SC(4,2)$ with various minimum p_T cuts ((a) and (c)) and results of normalized $SC(3,2)$ and $SC(4,2)$ ((b) and (d)) in Pb–Pb collisions at $\sqrt{s_{NN}} = 2.76 \text{ TeV}$. The panels (a) and (b) show the results for minimum p_T range $0.2 < p_T < 0.7 \text{ GeV}/c$ and the panels (c) and (d) are for minimum p_T range $0.8 < p_T < 1.5 \text{ GeV}/c$. Note that NSC data points from each minimum p_T in a centrality percentile bin are shifted for visibility.

as well as
225 and $SC(5,2)$ increase non-linearly toward peripheral collisions. In case of $SC(5,3)$ and $SC(4,3)$, the
226 centrality dependence is weaker than the other harmonic correlations and a monotonic increase is ob-
227 served for these harmonic correlations. NSC(5,3) shows the strongest correlation among all harmonics
228 while NSC(4,2), NSC(5,2) shows a weak centrality dependence. Both NSC(3,2) and NSC(4,3) show a
229 monotonic increase toward peripheral collisions with the similar magnitude.

To study the p_T dependence of $SC(m,n)$, we change the low p_T cut-off, instead of using independent
230 p_T intervals in order to avoid large statistical fluctuations in the results. Various minimum p_T cuts from
231 0.2 to 1.5 GeV/c are applied. The results of p_T dependence of $SC(3,2)$ and $SC(4,2)$ with minimum p_T
232 cuts $0.2 < p_T < 0.7 \text{ GeV}/c$ are shown on the panel (a) in Fig. 2a. The strength of $SC(m,n)$ becomes
233 larger as the minimum p_T increases. These p_T -dependent correlations have much stronger centrality de-
234 pendence, where $SC(m,n)$ gets much larger as the centrality or the minimum p_T cut increase. NSC(3,2)
235 and NSC(4,2) with different minimum cuts are shown on the panel (b) and (d) in Fig. 2b and 2d. The strong
236 p_T dependence observed in $SC(m,n)$ is not seen in NSC(m,n). The NSC(m,n) results are aligned all
237 together and consistent in errors for all minimum p_T cuts. This indicates that the p_T dependence of
238 $SC(m,n)$ is dominated by the p_T dependence of $\langle v_n \rangle$ values. The minimum p_T cuts are extended from
239 0.8 to 1.5 GeV/c and the results are shown on the panel (c) and (d) in Fig. 2c and 2d. While $SC(m,n)$ show the
240 similar trends as for $p_T < 0.8 \text{ GeV}/c$, NSC(m,n) tends to decrease with increasing p_T or the centrality.
241 The p_T dependence for NSC(3,2) is not clearly seen and it is consistent with no p_T dependence within the
242 current statistical and systematic errors for the centrality range $< 30\%$ and shows moderate decreasing
243 trend for increasing p_T for the $> 30\%$ centrality range. NSC(4,2) shows a moderate decreasing trend as p_T
244 or the centrality increases. These observations are strikingly different from p_T dependence of individual
245 flow harmonics, where the relative flow fluctuations $\sigma_{v_2}/\langle v_2 \rangle$ [51] are independent of momentum up to
246 $p_T \sim 8 \text{ GeV}/c$ (see Fig. 3 in Ref. [52]).

* I'm not sure we can describe values getting more negative
(i.e. decreasing) as "monotonically increasing". Perhaps this
paragraph could be reformulated in terms of "getting
more (anti)correlated" or something like that

248 6 Model Comparisons

249 We have compared the centrality dependence of our observables with the event-by-event EKRT+viscous
 250 hydrodynamic calculations [30], where the initial energy density profiles are calculated using a next-
 251 to-leading order perturbative-QCD+saturation model [53, 54]. The subsequent spacetime evolution is
 252 described by relativistic dissipative fluid dynamics with different parameterizations for the temperature
 253 dependence of the shear viscosity to entropy density ratio $\eta/s(T)$. This model gives a good description
 254 of the charged hadron multiplicity and the low p_T region of the charged hadron spectra at RHIC and
 255 the LHC (see Figs. 11–13 in [30]). Each of the $\eta/s(T)$ parameterizations is adjusted to reproduce the
 256 measured v_n from central to mid-peripheral collisions (see Fig. 14 in [30]).

257 The VISH2+1 [55, 56] event-by-event calculations for relativistic heavy-ion collisions are based on
 258 (2+1)-dimensional viscous hydrodynamics which describes both the QGP phase and the highly dis-
 259 sipative and even off-equilibrium late hadronic stage with fluid dynamics. With well-tuned transport
 260 coefficients and decoupling temperature, and given initial condition discussed later, it can describe the p_T
 261 spectra and different flow harmonics at RHIC and the LHC [5, 55, 57, 58]. Three different initial con-
 262 ditions (MC-Glauber, MC-KLN and AMPT) along with different constant η/s values are used in the
 263 model [39]. Traditionally, the Glauber model constructs the initial entropy density from contributions
 264 from of the wounded nucleon and binary collision density profiles [59], and the KLN model assumes that
 265 the initial entropy density is proportional to the initial gluon density calculated from the corresponding
 266 k_T factorization formula [60]. In the Monte Carlo versions (MC-Glauber and MC-KLN) [61–63], ad-
 267 dditional initial state fluctuations are introduced through the position fluctuations of individual nucleons
 268 inside the colliding nuclei. For the AMPT initial conditions [58, 64, 65], the fluctuating energy density
 269 profiles are constructed from the energy decompositions of individual partons, which fluctuate in both
 270 momentum and position coordinate. Compared with the MC-Glauber and MC-KLN initial conditions,
 271 the additional Gaussian smearing in the AMPT initial conditions gives rise to non-vanishing initial local
 272 flow velocities [64].

273 The centrality dependence of NSC observables is compared to that in the AMPT model [66–68]. Even
 274 though thermalization could be achieved in collisions of very large nuclei and/or at extremely high en-
 275 ergy [69], the dense matter created in heavy-ion collisions may not reach full thermal or chemical equi-
 276 librium as a result of its finite volume and short time scale. To address such non-equilibrium many-body
 277 dynamics, AMPT has been developed, which includes both initial partonic and final hadronic interac-
 278 tions and the transition between these two phases of matter. For the initial conditions, the AMPT model
 279 uses the spatial and momentum distributions of hard minijet partons and soft strings from the HIJING
 280 model [47, 70]. The AMPT model can be run in two main configurations, the default and the string
 281 melting model¹. In the default version, partons are recombined with their parent strings when they stop
 282 interacting. The resulting strings are later converted into hadrons using the Lund string fragmentation
 283 model [71, 72]. In the string melting version, the initial strings are melted into partons whose interactions
 284 are described by the ZPC parton cascade model [73]. These partons are then combined into the final state
 285 hadrons via a quark coalescence model. In both configurations, the dynamics of the subsequent hadronic
 286 matter is described by a hadronic cascade based on A Relativistic Transport (ART) model [74] which also
 287 includes resonance decays. The third version used in this article is based on the string melting configura-
 288 tion in which the hadronic rescattering phase is switched off to study its influence on the development of
 289 anisotropic flow. Even though the string melting version of AMPT [68, 75] reasonably reproduces par-
 290 ticle yields, p_T spectra, and v_2 of low- p_T pions and kaons in central and mid-central Au–Au collisions
 291 at $\sqrt{s_{NN}} = 200$ GeV and Pb–Pb collisions at $\sqrt{s_{NN}} = 2.76$ TeV [76], it was seen clearly in the recent
 292 study [77] that it fails to quantitatively reproduce the harmonic flow coefficients of identified hadrons
 293 (v_2, v_3, v_4 and v_5) at $\sqrt{s_{NN}} = 2.76$ TeV. It turns out that the radial flow in AMPT is 25% lower than the that

¹The input parameters used in both configurations are: $\alpha_s = 0.33$, a partonic cross-section of 1.5 mb, while the Lund string fragmentation parameters were set to $\alpha = 0.5$ and $b = 0.9$ GeV⁻².

294 measured value at the LHC, which indicates that the unrealistically low radial flow in AMPT is responsible
 295 for the quantitative disagreement [77]. The details of configurations of AMPT settings used for this
 296 article and the comparisons of p_T -differential v_n for pions, kaons and protons to the data can be found in
 297 [77].

298 6.1 Low Order Harmonic Correlations

299 SC(3,2) and SC(4,2) are compared to several theoretical calculations. The event-by-event EKRT+viscous
 300 hydrodynamic predictions with the different parameterizations for the temperature dependence of the
 301 shear viscosity to entropy density ratio $\eta/s(T)$ are shown in Fig. 2 of Ref. [38]. It has been demon-
 302 strated that NSC(3,2) observable is sensitive mainly to the initial conditions, while NSC(4,2) observable
 303 is sensitive to both the initial conditions and the system properties, which is consistent with the predic-
 304 tions from [21]. However, the sign of NSC(3,2) is positive in the models in 0-10% central collisions
 305 while it is negative in data. In the most central collisions the anisotropies originate mainly from fluctua-
 306 tions, i.e. the initial ellipsoidal geometry characteristic for mid-central collisions plays little role in this
 307 regime. This observation helps to understand better the fluctuations in initial energy density. NSC(4,2)
 308 observable shows better sensitivity for different $\eta/s(T)$ parameterizations but the model cannot describe
 309 either neither the centrality dependence nor the absolute values. This observed distinct discrepancy between
 310 data and theoretical predictions indicates that the current understanding of initial conditions used to
 311 model the initial stages of heavy-ion collision need to be revisited to further constrain the $\eta/s(T)$, con-
 312 sidering the difficulties in separating the role of the η/s from the initial conditions to the final state
 313 particle anisotropies [4, 25]. The use of SC(m, n) and NSC(m, n) can provide new constraints on the
 314 detailed modeling of fluctuating initial conditions. The better constraints on the initial state conditions
 315 will certainly reduce the uncertainties of determining $\eta/s(T)$.

316 The results with the comparison to VISH2+1 calculation [39] are shown in Fig. 3. All calculations with
 317 large η/s regardless of the initial conditions ($\eta/s = 0.2$ for MC-KLN and MC-Glauber initial conditions
 318 and $\eta/s = 0.16$ for AMPT initial conditions) fail to capture the centrality dependence of SC(3,2) and
 319 SC(4,2). Among the calculations with small η/s ($\eta/s = 0.08$), the one with the AMPT initial conditions
 320 describes the data better both for SC(3,2) and SC(4,2) in general but it cannot describe the data quan-
 321 titatively for most of the centrality ranges. Similarly to the event-by-event EKRT+viscous hydrodynamic
 322 calculations [30], the sign of the normalized NSC(3,2) in the model calculations in Fig 3 is opposite
 323 to that in data in 0-10% central collisions. NSC(3,2) does not show sensitivity to the initial conditions
 324 nor to the different η/s parameterizations used in the models and cannot be described by these models
 325 quantitatively. However, NSC(4,2) is sensitive both to the initial conditions and the η/s parameteriza-
 326 tions used in the models. Even though NSC(4,2) favors both AMPT initial conditions with $\eta/s = 0.08$
 327 and MC-Glauber initial conditions with $\eta/s = 0.20$, SC(4,2) can be only described by smaller η/s from
 328 AMPT and MC-Glauber initial conditions. Hence the calculations with large $\eta/s = 0.20$ is ruled out.
 329 We conclude that η/s should be small and AMPT initial condition is favored by the data.

330 The SC(m, n) calculated from AMPT simulations are compared to data in Fig. 4. As for SC(3,2), none
 331 of the calculations can describe the data and the calculation with the default AMPT setting follows the
 332 trend of the data closest. The same default calculation can describe the sign and magnitude of NSC(3,2)
 333 while the hydrodynamic calculations failed to describe the sign and magnitude of the observable in the
 334 most central collisions. Interestingly, the string melting AMPT model cannot reproduce the data and
 335 the strength of the correlations are weaker than in data. The third version based on the string melting
 336 configuration without the hadronic rescattering phase is also shown. The hadronic rescattering stage
 337 makes both SC(3,2) and NSC(3,2) stronger in the string melting AMPT model but not enough to describe
 338 the data. Further we investigated why the default AMPT model can describe NSC(3,2) fairly well but
 339 underestimates SC(3,2). By taking the differences in the individual flow harmonics (v_2 and v_3) between
 340 the model and data into account, we were able to recover the difference in SC(3,2) between the data
 341 and the model. The discrepancy in SC(3,2) can be explained by the overestimated individual v_n values as

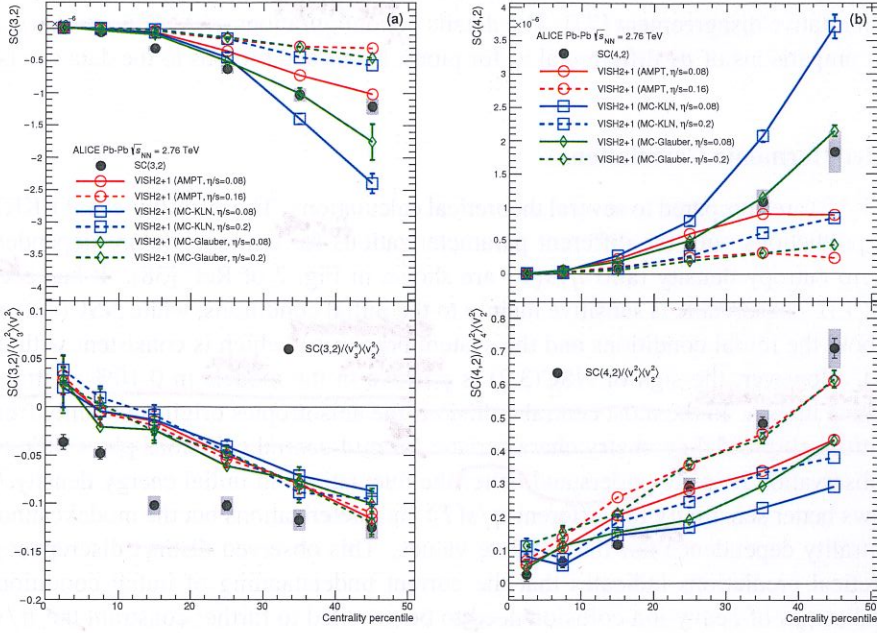


Fig. 3: SC(3,2) (a) and SC(4,2) (b) in Pb–Pb collisions at $\sqrt{s_{NN}} = 2.76$ TeV are compared to various VISH2+1 calculations [39] with different settings. Upper (lower) panels show SC(m,n) (NSC(m,n)). Calculations with three initial conditions from AMPT, MC-KLN, and MC-Glauber are drawn as different colors and markers. The η/s parameters are shown in line styles, the small $\eta/s = 0.08$ are shown as solid lines, and large $\eta/s > 0.2$ for MC-KLN and MC-Glauber, 0.16 for AMPT are drawn as dashed lines.

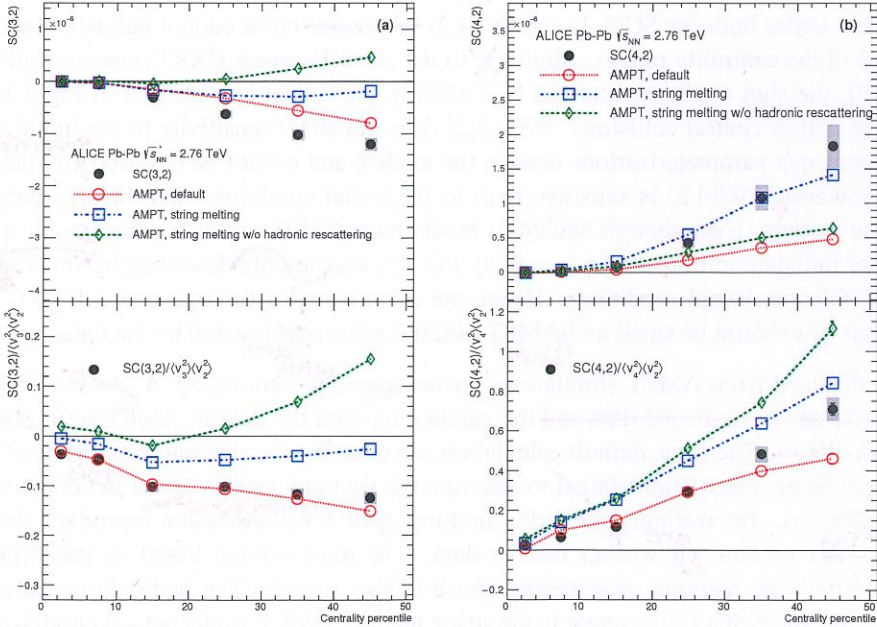
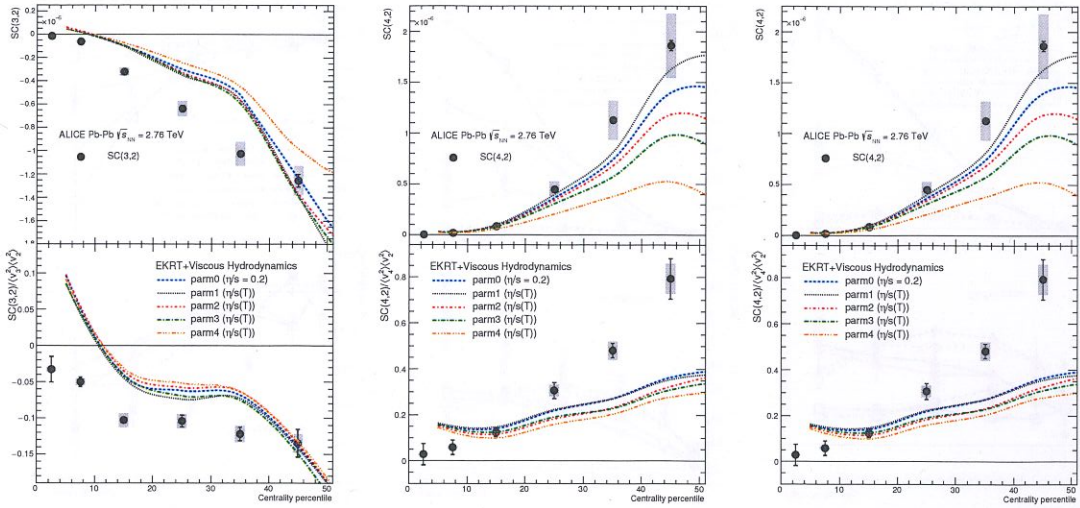


Fig. 4: SC(3,2) (a) and SC(4,2) (b) in Pb–Pb collisions at $\sqrt{s_{NN}} = 2.76$ TeV are compared to various AMPT models. Upper panels (lower) are the results of SC(m,n) (NSC(m,n)).



Measurements

Fig. 5: Results of $SC(5,2)$, $SC(5,3)$ and $SC(4,3)$ in $Pb-Pb$ collisions at $\sqrt{s_{NN}} = 2.76$ TeV are compared to the event-by-event EKRT+viscous hydrodynamic calculations [30]. The dashed lines are hydrodynamic predictions with various $\eta/s(T)$ parameterizations [30]. These $SC(3,2)$ and $SC(4,2)$ will be replaced with new figures for higher order correlations once we have the calculations from Harri Niemi et. al [30].

reported in [77] in all the centrality ranges.

In the case of $SC(4,2)$, the string melting AMPT model can fairly well describe the data while the default model underestimates it. NSC($4,2$) is slightly overestimated by the same setting which can describe $SC(4,2)$ but the default AMPT model can describe the data better. The influence of the hadronic rescattering phase for NSC($4,2$) is opposite to other observables ($SC(3,2)$, NSC($3,2$) and $SC(4,2)$). The hadronic rescattering makes NSC($4,2$) slightly smaller. It should be noted that the better agreement for $SC(m, n)$ should not be overemphasized since there are discrepancies in the individual v_n between the AMPT models and the data as it was demonstrated for $SC(3,2)$. Hence the simultaneous description of $SC(m, n)$ and NSC(m, n) should give better constraints to the parameters in AMPT models.

6.2 Higher Order Harmonic Correlations

The higher order harmonic correlations ($SC(4,3)$, $SC(5,2)$ and $SC(5,3)$) are compared to several theoretical calculations. The event-by-event EKRT+viscous hydrodynamic predictions with the different parameterizations for the temperature dependence of the shear viscosity to entropy density ratio $\eta/s(T)$ are shown in Fig. 5. [Waiting for $\eta/s(T)$ hydro calculations from Harri Niemi et. al [30], figure will be replaced later, just a place holder]

The higher order harmonic correlations ($SC(4,3)$, $SC(5,2)$ and $SC(5,3)$) are compared to VISH2+1 calculations [39], shown in Fig. 6. All the models with large η/s regardless of the initial conditions ($\eta/s = 0.2$ for MC-KLN and MC-Glauber initial conditions, and $\eta/s = 0.16$ for AMPT) failed to capture the centrality dependence of $SC(5,2)$, $SC(5,2)$ and $SC(5,3)$, more clearly than for the lower order harmonic correlations ($SC(3,2)$ and $SC(4,2)$). Among the models with small η/s ($\eta/s = 0.08$), the one from the AMPT initial condition describes the data much better than the ones with other initial conditions. A quite clear separation between different initial conditions is observed for these higher order harmonic correlations compared to the lower order harmonic correlations. NSC($5,2$) and $SC(5,3)$ are quite sensitive to both the initial conditions and the η/s parameterizations. Similarly as the above mentioned hydrodynamic calculations [30], the sign of the NSC($4,3$) in these models is opposite to its signature sign in the data in 0-10% central collisions. NSC($4,3$) shows sensitivity to both initial conditions and η/s

mentioned above

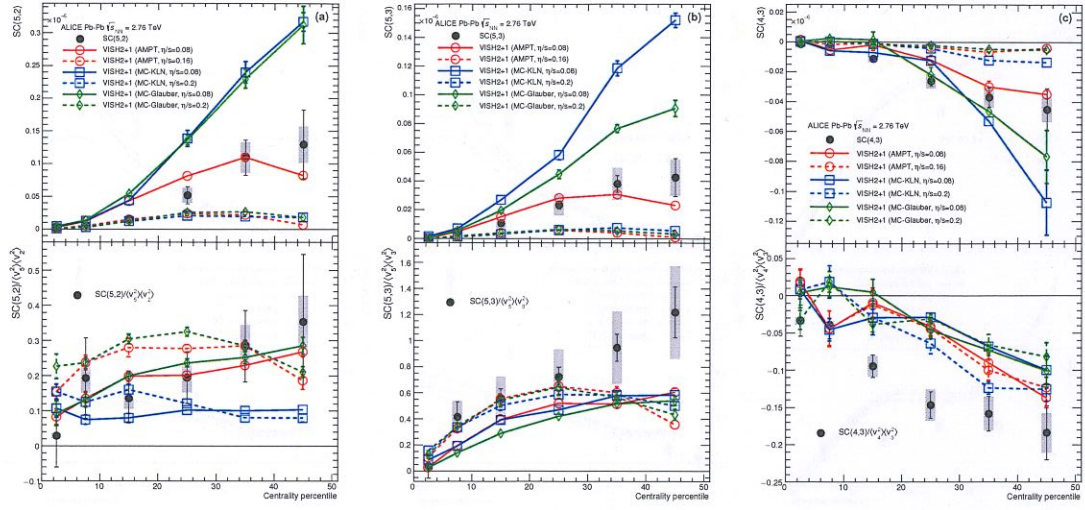


Fig. 6: Results of SC(5,2), SC(5,3) and SC(4,3) in Pb–Pb collisions at $\sqrt{s_{\text{NN}}} = 2.76 \text{ TeV}$ are compared to various VISH2+1 calculations [39]. Three initial conditions from AMPT, MC-KLN and MC-Glauber are drawn as different colors and markers. The η/s parameters are shown as different line styles, the small shear viscosity ($\eta/s = 0.08$) are shown as solid lines, and large shear viscosities ($\eta/s = 0.2$ for MC-KLN and MC-Glauber, 0.16 for AMPT) are drawn as dashed lines. Upper panels are the results of $\text{SC}(m,n)$ and lower panels are the results of $\text{NSC}(m,n)$.

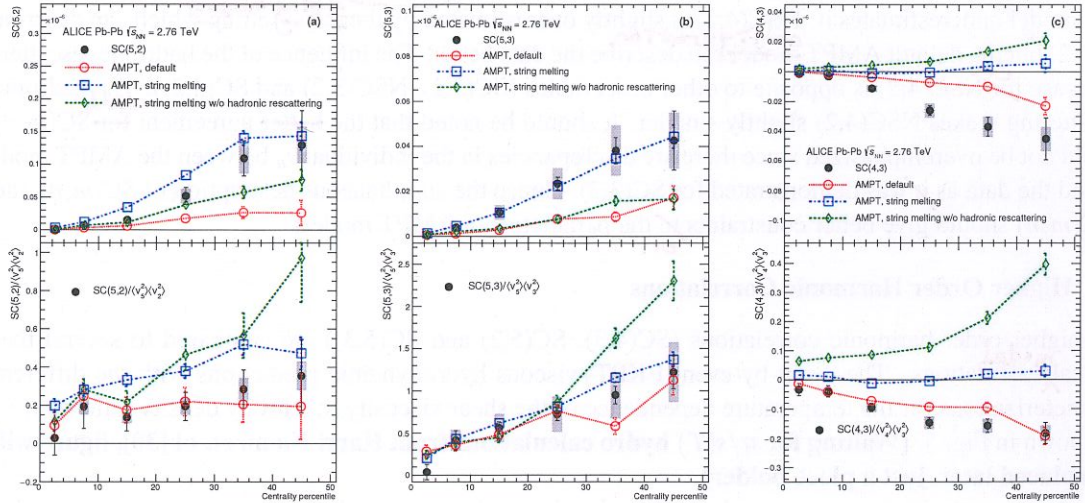


Fig. 7: Results of SC(5,2), SC(5,3) and SC(4,3) in Pb–Pb collisions at $\sqrt{s_{\text{NN}}} = 2.76 \text{ TeV}$ are compared to various AMPT models. Upper panels are the results of $\text{SC}(m,n)$ and the lower panels are the results of $\text{NSC}(m,n)$.

parameterizations. The ~~SC(4,3) data is clearly favored by smaller η/s~~ but NSC(4,3) cannot be described by these models quantitatively.

The extracted results for final state particles from AMPT simulations in the same way as for the data are compared in Fig. 7. The string melting AMPT model describes SC(5,3) and NSC(5,3) well. However, the same setting overestimates SC(5,2) and NSC(5,2). However, the default AMPT model can describe NSC(5,3) and NSC(5,2) fairly well as it is the case for NSC(3,2) and NSC(4,2) seen in Fig. 4. In the in the case of the lower harmonics

case of SC(4,3), neither of the settings can describe the data but the default AMPT model follows the data ~~closest~~. The string melting AMPT model fails to describe SC(4,3) and NSC(4,3). In summary, the default AMPT model describes well the normalized symmetric cumulants (NSC(m, n)) from lower to higher order harmonic correlations while the string melting AMPT model overestimates NSC(5,2) and underestimates (or predicts very weak correlation) NSC(4,3).

As discussed in Sec. 5, a hierarchy NSC(5,3) > NSC(4,2) > NSC(5,2) holds for centrality ranges > 20% within the errors and NSC(5,2) is smaller than NSC(5,3) while SC(5,2) is larger than SC(5,3). Except for 0-10% centrality range, we found that the same hierarchy also holds for the hydrodynamic calculations and the AMPT models in this article. The observed difference between SC(5,2) and NSC(5,3) (SC(5,2) > SC(5,3)) can be explained by the difference of magnitudes. This can be attributed to the fact that the flow fluctuation is stronger for v_3 than v_2 [78]. It was claimed in Ref. [39] and seen also in Ref. [79] based on a AMPT model. NSC(m, n) correlators increase with the larger η/s in hydrodynamic calculations in 0-30% centrality range in the same way as the event plane correlations [80, 81]. In semi-peripheral collisions (>40%), the opposite trend is observed.

We list here important findings from the model comparisons:

- (i) The NSC(3,2) observable is sensitive mainly to the initial conditions, while NSC(4,2) observable is sensitive to both the initial conditions and the temperature dependence of η/s .
- (ii) All the VISH2+1 model calculations with large η/s regardless of the initial conditions failed to capture the centrality dependence of correlations.
- (iii) Among the VISH2+1 model calculations with small η/s ($\eta/s = 0.08$), the one with the AMPT initial condition describes the data better in general but it cannot describe the data quantitatively for most of the centrality ranges.
- (iv) The correlation strength of v_3 and v_2/v_4 and v_3 (NSC(3,2) and NSC(4,3)) is underestimated in hydrodynamic model calculations.
- (v) The sign of NSC(3,2) in 0-10% central collisions was found to be different between the data and the hydrodynamic model calculations while the default AMPT model can reproduce the sign.
- (vi) The default AMPT model can describe the normalized symmetric cumulants (NSC(m, n)) quantitatively for most of centralities while the string melting AMPT model fails to describe them.
- (vii) A hierarchy NSC(5,3) > NSC(4,2) > NSC(5,2) holds for centrality ranges > 20% within the errors. This hierarchy is well reproduced both by hydrodynamic and AMPT model calculations.

6.3 Transverse Momentum Dependence of Correlations between v_2 , v_3 and v_4

It can be seen in Fig. 2 that the p_T dependence for NSC(3,2) is not clearly seen and it is consistent with no p_T dependence for the centrality range < 30%, and shows moderate decreasing trend for increasing p_T for > 30% centrality range. NSC(4,2) shows a moderate decreasing trend as p_T or the centrality increase. In order to see the trend more clearly, we show NSC(m, n) results as a function of minimum p_T cut in Fig. 8.

NSC(3,2) and NSC(4,2) as a function of different minimum p_T cut are compared to the AMPT simulations in Fig. 8. The observed p_T dependence for NSC(3,2) and NSC(4,2) in mid-central collisions is seen also in AMPT simulations for higher minimum p_T cuts. The other AMPT configurations except for the default AMPT model give very strong p_T dependence above 1 GeV/c and cannot describe the magnitude of the data both for NSC(3,2) and NSC(4,2) simultaneously. In the case of NSC(3,2), the

With the exception of the default settings configuration,

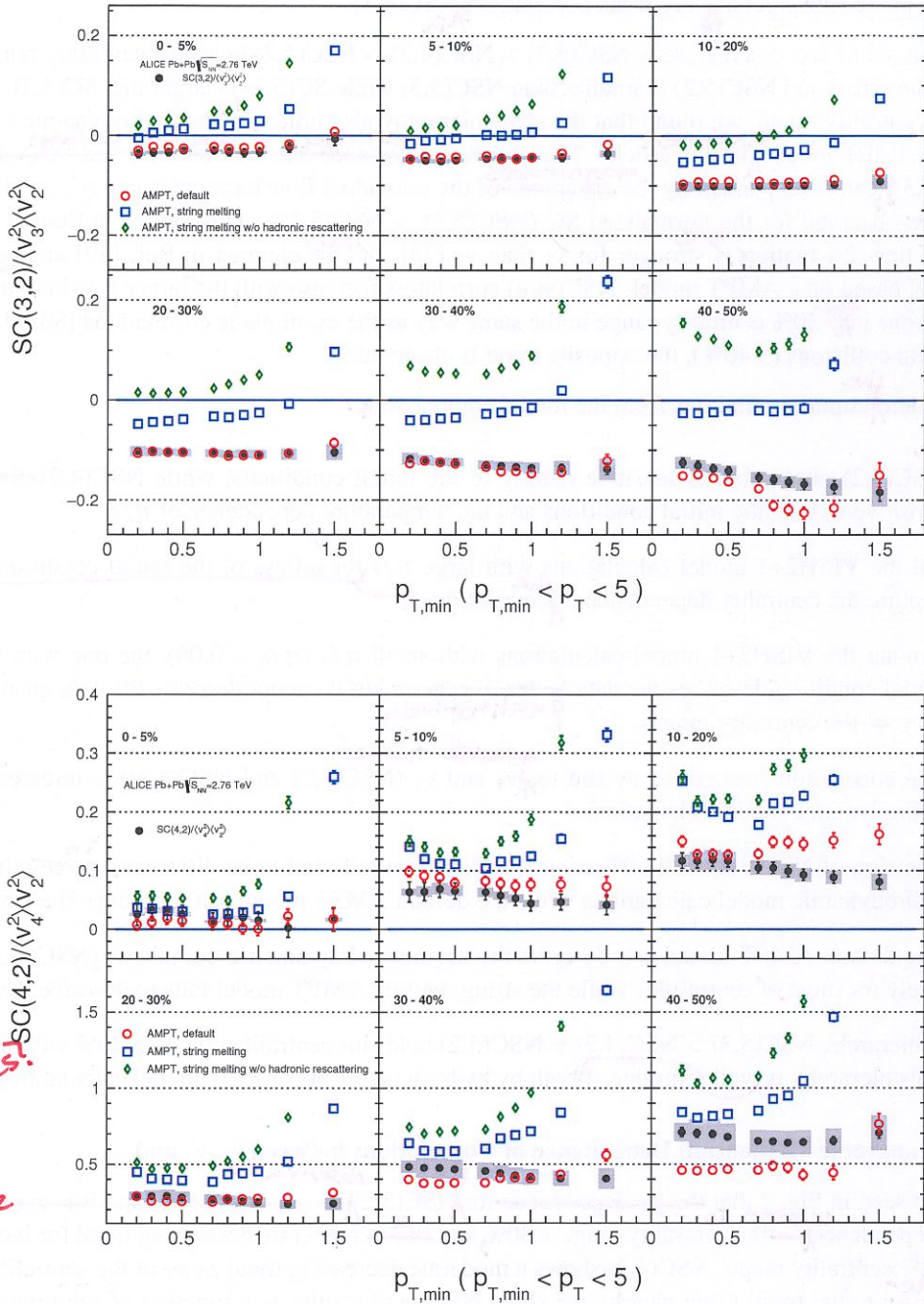


Fig. 8: NSC(3,2) (Top) and NSC(4,2) (Bottom) as a function of minimum p_T cuts in Pb–Pb collisions at $\sqrt{s_{\text{NN}}} = 2.76 \text{ TeV}$ are compared to various AMPT models.

416 default AMPT model describes the magnitude and p_T dependence well in all collision centralities except
 417 for 40 – 50% where the model underestimates the data and shows a stronger p_T dependence than the data.
 418 As for NSC(4,2), the same model which describes NSC(3,2) also can reproduce the data well except for
 419 10 – 20% and 40 – 50% centralities where some deviations from the data both for the magnitude and p_T
 420 dependence are observed. When the string melting AMPT model is compared to the same model with
 421 the hadronic rescattering off, it is observed that the very strong p_T dependence as well as the correlation
 422 strength get weaker by the hadronic rescattering. This might imply that the hadronic interactions are
 423 the source of this observed p_T dependence even though the relative contributions from partonic and hadronic
 424 stage in the final state particle distributions should be studied further. This observed moderate p_T dependence in mid-
 425 central collisions both for NSC(3,2) and NSC(4,2) might be an indication of possible viscous corrections
 426 for the equilibrium distribution at hadronic freeze-out predicted in [37]. The comparisons to hydro-
 427 dynamic models can further help to understand the viscous corrections to the momentum distribution at
 428 hadronic freeze-out [30, 36].

429 7 Summary

430 In this article, we report the centrality dependence of correlations between the higher order harmonics
 431 (v_3, v_4, v_5) and the lower order harmonics (v_2, v_3) as well as the transverse momentum dependence of
 432 v_3-v_2 and v_4-v_2 correlations. The results are obtained with Symmetric 2-harmonic 4-particle Cumulants (SC).
 433 It was demonstrated earlier in [38] that this method is insensitive to the non-flow effects and free
 434 from symmetry plane correlations. We have found that fluctuations of v_3-v_2 and v_4-v_3 are anti-correlated
 435 in all centralities while fluctuations of v_4-v_2, v_5-v_2 and v_5-v_3 are correlated for all centralities. This mea-
 436 surement were compared to various hydrodynamic model calculations with different initial conditions as
 437 well as different parameterizations of the temperature dependence of η/s . It is found that the different
 438 order harmonic correlations have different sensitivities to the initial conditions and the system properties.
 439 Therefore they have discriminating power in separating the effects of η/s from the initial conditions to on
 440 the final state particle anisotropies. The sign of v_3-v_2 correlation in 0-10% central collisions was found
 441 to be different between the data and hydrodynamic model calculations. In the most central collisions the
 442 anisotropies originate mainly from fluctuations, where the initial ellipsoidal geometry which dominates
 443 in mid-central collisions plays little role. This observation might help to understand the details of the
 444 fluctuations in initial conditions. The comparisons to VISH2+1 calculation show that all the models with
 445 large η/s , regardless of the initial conditions failed to capture the centrality dependence of higher order
 446 correlations, more clearly than lower order harmonic correlations. Based on the tested model parameters,
 447 the η/s should be small and AMPT initial condition is favored by the data. A quite clear separation of
 448 the correlation strength between different initial conditions is observed for these higher order harmonic
 449 correlations compared to the lower order harmonic correlations. The default configuration of AMPT
 450 model describes well the normalized symmetric cumulants (NSC(m,n)) for most of centralities and for
 451 most combinations of harmonics which were considered. Together with the measurements of individual
 452 harmonics these results provide further constraints on the system properties and help discriminating be-
 453 tween theoretical models. Finally, we have found that v_3 and v_2-v_4 and v_2 correlations have moderate
 454 p_T dependence in mid-central collisions. This might be an indication of possible viscous corrections for to
 455 the equilibrium distribution at hadronic freeze-out. The results presented in this article can be used to
 456 further optimize model parameters and put better constraints on the initial conditions and the transport
 457 properties of nuclear matter in ultra-relativistic heavy-ion collisions.

458 Acknowledgements

459 References

- 460 [1] STAR Collaboration, K. H. Ackermann *et al.*, ‘Elliptic flow in Au + Au collisions at